

# 1 Accurate and robust inference of 2 genetic ancestry from 3 cancer-derived molecular data 4 across genomic platforms

5 **Pascal Belleau**<sup>1,2</sup>, **Astrid Deschênes**<sup>2,3</sup>, **David A. Tuveson**<sup>2,3</sup>, and **Alexander**  
6 **Krasnitz**<sup>1,2\*</sup>

\*For correspondence:  
[krasnitz@cshl.edu](mailto:krasnitz@cshl.edu) (AK)

7 <sup>1</sup>Simons Center for Quantitative Biology, Cold Spring Harbor Laboratory, Cold Spring  
8 Harbor, New York, USA; <sup>2</sup>Cancer Center, Cold Spring Harbor Laboratory, Cold Spring  
9 Harbor, New York, USA; <sup>3</sup>Lustgarten Foundation Pancreatic Cancer Research  
10 Laboratory, Cold Spring Harbor, New York, USA

---

12 **Abstract** Genetic ancestry-oriented cancer research requires the ability to perform accurate  
13 and robust ancestry inference from existing cancer-derived data, including whole exomes,  
14 transcriptomes and targeted gene panels, very often in the absence of matching cancer-free  
15 genomic data. In order to optimize and assess the performance of the ancestry inference for any  
16 given input cancer-derived molecular profile, we develop a data synthesis framework. In its core  
17 procedure, the ancestral background of the profiled patient is replaced with one of any number  
18 of individuals with known ancestry. Data synthesis is applicable to multiple profiling platforms  
19 and makes it possible to assess the performance of inference separately for each  
20 continental-level ancestry. This ability extends to all ancestries, including those without  
21 statistically sufficient representation in the existing cancer data. We further show that our  
22 inference procedure is accurate and robust in a wide range of sequencing depths. Testing our  
23 approach for three representative cancer types, and across three molecular profiling modalities,  
24 we demonstrate that global, continental-level ancestry of the patient can be inferred with high  
25 accuracy, as quantified by its agreement with the golden standard of the ancestry derived from  
26 matching cancer-free molecular data. Our study demonstrates that vast amounts of existing  
27 cancer-derived molecular data potentially are amenable to ancestry-oriented studies of the  
28 disease, without recourse to matching cancer-free genomes or patients' self-identification by  
29 ancestry.

---

## 31 **Keywords**

32 genetic ancestry, cancer, secondary data analysis

## 33 **Introduction**

34 There is ample epidemiological evidence that race and/or ethnicity are important determinants of  
35 incidence, clinical course and outcome in multiple types of cancer (*Siegel et al., 2020; Cronin et al.,*  
36 *2018; Ashktorab et al., 2017; Huang et al., 2019; Tan et al., 2016*). As such, these categories must  
37 be taken into account in the analysis of molecular data derived from cancer. A number of recently  
38 published large-scale genomic studies of cancer (*Mahal et al., 2020; Carrot-Zhang et al., 2020; Yuan*

39 *et al., 2018; Sinha et al., 2020; Bhatnagar et al., 2021; Carrot-Zhang et al., 2021*) point to differences  
40 in the molecular make-up of the disease among groups of different ancestral background and to  
41 the need for more molecular data to power discovery of such differences.

42 Ancestry annotation of cancer-derived data largely draws on two sources. One is a patient's  
43 self-identified race and/or ethnicity (SIRE). SIRE is often missing, sometimes inaccurate and usually  
44 incomplete. As a recent analysis (*Nugent et al., 2019*) of PubMed database entries since 2010  
45 reveals, patients' SIRE is massively under-reported in genome and exome sequencing studies of  
46 cancer, with only 37% of these reporting race, and 17% reporting ethnicity. Furthermore, SIRE is  
47 not always consistent with genetic ancestry. Finally, a self-declaring patient is often given a choice  
48 from a small number of broad racial or ethnic categories, which fail to capture complete ancestral  
49 information, especially in cases of mixed ancestry (*Mersha and Abebe, 2015*).

50 A far more accurate and detailed ancestral characterization may be obtained by genotyping  
51 a patient's DNA from a cancer-free tissue. Powerful methods exist for ancestry inference from  
52 germline DNA sequence (*Pritchard et al., 2000; Price et al., 2006; Alexander et al., 2009; Diaz-  
53 Papkovich et al., 2019*). These methods were recently used to determine ancestry of approxi-  
54 mately 10,000 patients profiled by The Cancer Genome Atlas (TCGA) (*Carrot-Zhang et al., 2020;  
55 Yuan et al., 2018*). However, genotyping of DNA from patient-matched cancer-free specimens is  
56 not part of standard clinical practice, where the purpose of DNA profiling is often identification  
57 of mutations with known oncogenic effects, such as those in the Catalog Of Somatic Mutations In  
58 Cancer (COSMIC) database (*Tate et al., 2018*). As a result, it is not performed routinely outside aca-  
59 demic clinical centers or major research projects. There also are studies yielding sequence data  
60 from tumors, whose purpose does not require germline profiling. RNA sequencing (RNA-seq) for  
61 expression quantification is in this category. Finally, peripheral blood is most often the source of  
62 germline DNA in the clinic, but this is not always the case for diseases of the hematopoietic system,  
63 such as leukemia, wherein cancer cells are massively present in circulation. In summary, matched  
64 germline DNA sequence is not universally available for cancer-derived molecular data. In such  
65 cases, it is necessary to infer ancestry from the nucleic acid sequence of the tumor itself.

66 Standard methods of ancestry inference commonly rely on population specificity of germline  
67 single-nucleotide variants (SNV). Whole-genome (WGS) or whole-exome sequences (WES), at depths  
68 sufficient for reliably calling single-nucleotide variants, and readouts from genotyping microarrays,  
69 are therefore data types most suitable for this purpose. However, such detailed DNA profiling is  
70 often not performed in molecular studies of cancer. In such cases, it is necessary to infer ancestry  
71 from other types of tumor-derived data, including RNA sequence and DNA sequence for a small  
72 panel of genes, e.g., FoundationOne® CDx (*Frampton et al., 2013*).

73 For all types of tumor-derived sequence, accurate inference of ancestry is a potential challenge.  
74 Tumor genome is often replete with somatic alterations, including loss of heterozygosity (LOH),  
75 copy number variants (CNV), translocations, microsatellite instabilities and SNV. Of these, struc-  
76 tural variants, especially LOH and CNV, are the most likely to affect the genetic ancestry calls, but  
77 other types of alterations also are, to various degrees, potential obstacles to accurate ancestry  
78 inference. Tumor RNA-seq presents additional challenges, namely, extremely uneven coverage of  
79 the transcript due to a broad range of RNA expression levels and distortions due to allele-specific  
80 expression. Gene panels represent a very small fraction of the genome, whose sufficiency for an-  
81 cestry inference is not clear and may vary from panel to panel. In addition, cancer gene panels are  
82 enriched in cancer driver genes, which tend to undergo somatic alteration more frequently than  
83 other parts of the genome.

84 Important recent publications on ancestral effects in cancer reported patient ancestry inferred  
85 from matching cancer-free DNA (*Carrot-Zhang et al., 2020; Yuan et al., 2018; Carrot-Zhang et al.,  
86 2021*). At the same time, there has been much less work on ancestry inference from tumor-derived  
87 nucleic acids. A recent analysis of tumor genomes from TCGA and GEO repositories, profiled by  
88 SNP microarrays, demonstrated a high degree of coincidence between patient ancestries inferred  
89 from these data and those inferred from SNP profiles of matching germline genomes (*Huang and*

90 *Baudis, 2020*). This study did not report inference results from other molecular profiling modalities.  
91 Similar agreement has been found, for a set of over 300 cancer cell lines, between the self-declared  
92 race/ethnicity of the donors and ancestry inferred from the SNP array data (*Yuan et al., 2018*), but  
93 that finding was not validated against matching cancer-free data. Ancestry was also inferred in  
94 two large collections of cancer cell lines using SNP microarray data (*Dutil et al., 2019; Kessler et al.,*  
95 *2019*). In the absence of matching cancer-free genotypes or self-declared ancestry of the donor  
96 the inference accuracy could not be assessed in these two studies. Ancestry inference from RNA  
97 sequences, 174 of which were derived from cancer tissue specimens, was considered in a recent  
98 study (*Barral-Arca et al., 2019*). However, these inferred ancestries were neither compared to  
99 ancestry calls from germline sequence nor to self-declared ancestries for accuracy assessment.  
100 Ancestry has been inferred for a large set of patient cases profiled with the FoundationOne® CDx  
101 gene panel (*Frampton et al., 2013*), but these ancestry calls were neither compared to those from  
102 the germline sequence nor to the patients' SIRE. A more recent study (*Carrot-Zhang et al., 2021*)  
103 compared, with encouraging results, ancestry inference from cancer-derived FoundationOne® CDx  
104 data to matching cancer-free ancestry calls, but this analysis was confined to lung cancer in mixed  
105 American super-population. To our knowledge, no systematic computational framework for an-  
106 cestry inference from cancer-derived molecular data, across assay and cancer types, has been  
107 developed to date. There is presently no ability to assess the inference accuracy specifically for  
108 a given input tumor-derived molecular profile with all its attendant properties, including the data  
109 quality and the depth of coverage. Reliable and accurate ancestry inference from tumor-derived  
110 nucleic acids thus represents an unmet need, which the present work aims to address.

111 For this purpose, we designed an inference procedure having in mind a scenario, likely to occur  
112 in studies of existing data or of archived tissue specimens, with an input molecular profile of a tu-  
113 mor from a single patient, and no matching cancer-free sequence available. The profile in question  
114 may have its unique set of sequence properties. These include the target sequence and uniformity  
115 of its coverage, depth, read length and sequencing quality. These profile-specific properties may be  
116 vastly dissimilar from those in the available public data sets with reliably known genetic ancestry of  
117 the patients. Furthermore, not all ancestries are equally easy to infer: for example, a Mixed Amer-  
118 ican ancestral category is sometimes difficult to distinguish either from African or from European  
119 ancestry. This profile specificity would make it impossible to confidently assess the accuracy of the  
120 inference procedure for the input profile from its performance with the public cancer-derived data  
121 in aggregate. In order to overcome this difficulty, we develop a computational technique, which is  
122 described schematically in *Figure 1* wherein the ancestral background of the patient is supplanted  
123 in the input profile by one of an unrelated individual with known ancestry. We next apply estab-  
124 lished methods of ancestry inference to this synthetic profile and compare the result to that known  
125 ancestry. Generating multiple such synthetic profiles allows us to assess how accurate the ancestry  
126 inference is for the patient, both overall and as a function of the profile's continental-level ancestry.  
127 Furthermore, using synthetic data, we are able to optimize the inference procedure with respect to  
128 parameters on which it depends. Importantly, this assessment and optimization procedure does  
129 not require the profile in question to be part of a larger data set from a cohort of patients with a  
130 similar diagnosis. Very often in public cancer-derived data, such cohorts do not provide statistically  
131 meaningful representation of non-European ancestries. This insufficiency is not an impediment to  
132 the application of our methodology.

133 In the following, we assess the accuracy of global ancestry calls from tumor exomes, narrowly  
134 targeted gene panels and RNA sequences, in comparison to such calls from matching germline  
135 genotypes, as profiled by exome sequencing or SNP microarrays. We do so for three cancer types,  
136 namely, pancreatic adenocarcinoma (PDAC) and ovarian cystadenocarcinoma (OV) as representa-  
137 tive types of epithelial tumors, and acute myeloid leukemia (AML), as an example of hematopoietic  
138 malignancy. Each of these data sets represents a unique challenge for patients' ancestry inference.  
139 OV is characterized by massive copy number alterations, often spanning much of the genome. Our  
140 PDAC data originate from patient-derived organoid (PDO) models of the disease (*Tiriak et al., 2018*).

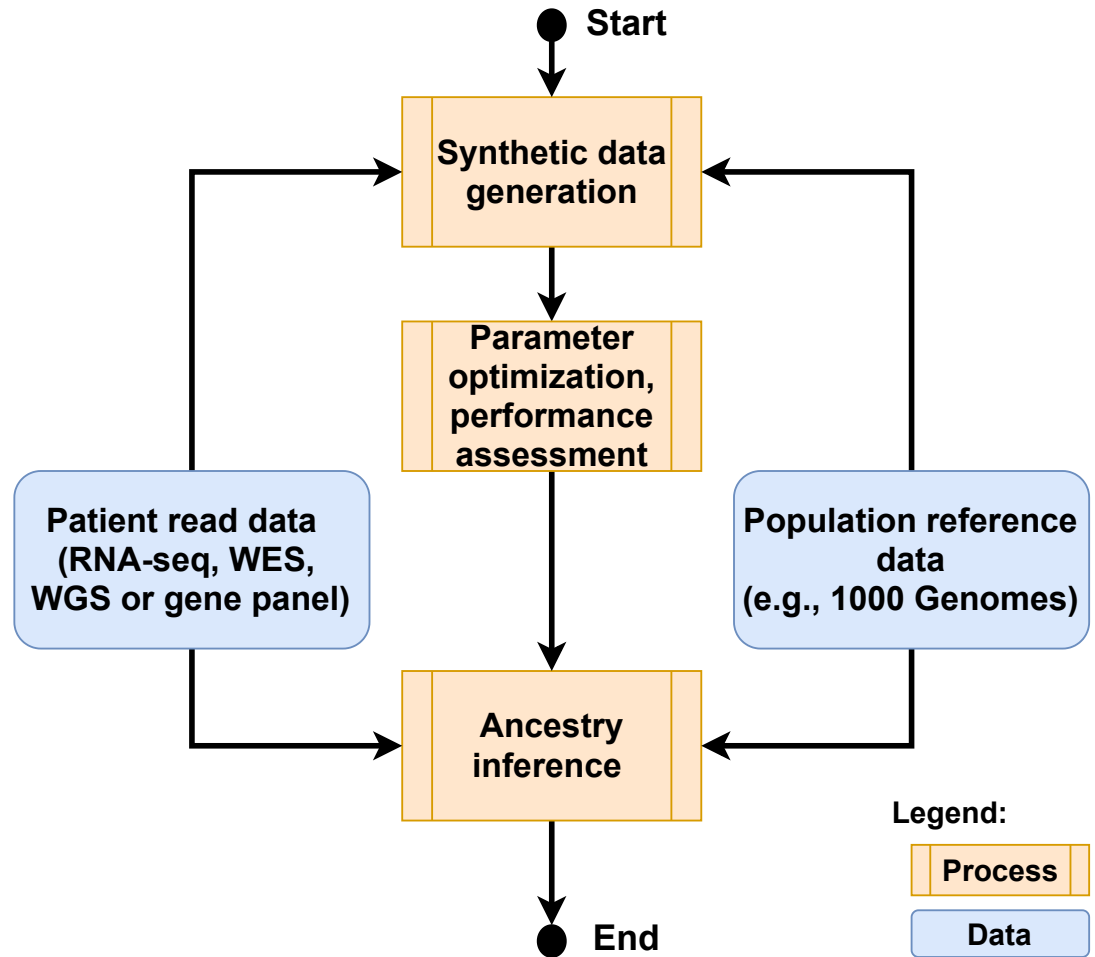


**Figure 1.** An overview of genetic ancestry inference from cancer-derived molecular data using data synthesis.

141 In PDO, near-100% tumor purity is achieved, exacerbating effects of copy number loss and loss of  
142 heterozygosity on the sequence. In AML the peripheral blood, the usual source of cancer-free DNA,  
143 may be severely contaminated by the cancer.

## 144 Results

145 We assessed the performance of genetic ancestry inference from three genomic data types: whole  
146 exomes, gene panels targeting exomes of several hundred cancer-related genes each and RNA se-  
147 quences. Throughout the study, we used the 1000 Genomes (1KG) data set, with no relatives for  
148 the individuals included (*Altshuler et al., 2010; Fairley et al., 2019*), as reference, against which pa-  
149 tient molecular data were compared to infer continental-level global ancestry. The latter is defined  
150 as a categorical variable taking five values: African (AFR), East Asian (EAS), European (EUR), Mixed  
151 American (AMR) and South Asian (SAS). These are called super-populations in the 1KG terminology.  
152 Each super-population comprises a number of subcontinental-level populations ( (*Fairley et al.,*  
153 *2019*)).

154 Our assessment relied on molecular data collected from three patient cohorts, each represent-  
155 ing a cancer type, namely, tissue donors to the Cold Spring Harbor Laboratory (CSHL) pancreatic  
156 ductal adenocarcinoma (PDAC) library of patient-derived organoids; acute myeloid leukemia (AML)  
157 patients enrolled in Beat AML clinical trial; and patients comprising TCGA ovarian cancer cohort  
158 (TCGA-OV) (*The Cancer Genome Atlas Research Network, 2011*). In these cohorts, patient molecu-  
159 lar data were available from tissue specimens both of cancer and cancer-free. *Figure 2* and Sup-  
160 plementary Table S2 contain a summary of molecular data underlying the study.

161 We employed principal-component analysis (PCA) as our inference tool of choice, and applied  
162 it as follows (*Figure 3*) (*Alexander et al., 2009*).

163 As a basis for the analysis, we used genotypes at genomic positions where single-nucleotide se-  
164 quence variants occurred with a frequency above a threshold in at least one super-population as  
165 sampled by 1KG. This basis was further reduced, for each individual cancer-derived molecular pro-  
166 file, to genotypes at positions with high sequence coverage by high-quality reads in the profile. We  
167 then computed singular-value decomposition of the reduced 1KG genotype matrix and projected  
168 the genotype of the cancer-derived profile onto the first  $D$  of the resulting principal components.  
169 The ancestry for the profile was determined as that of the majority among the nearest  $K$  1KG neigh-  
170 bors of the profile in this  $D$ -dimensional space (*Yuan et al., 2018*). For a subset of patients in each  
171 cohort we individually assessed the performance of the ancestry inference, as a function of the  
172 parameters  $D$  and  $K$ . This assessment was based, for each patient in the subset, on a large num-  
173 ber of synthetic cancer-derived molecular profiles, as outlined in the Introduction, schematically  
174 described in *Figure 5* and explained in greater detail in the Methods section. The result was quan-  
175 tified, for a given  $D, K$  pair of parameters, as the area under receiver operating characteristic (AU-  
176 ROC) (*Robin et al., 2011; Sun and Xu, 2014; Hand and Till, 2001*). Both super-population-specific and  
177 overall AUROC values were computed in a range of  $D, K$  pairs, as illustrated in *Figure 4* for 10 PDAC  
178 patients and AMR-specific AUROC (the similar figures for all the cohorts and super-populations are  
179 in *Figure S1*). Optimal  $D, K$  pairs maximizing the overall AUROC were chosen. From this subset of  
180 patients we observed, for each cancer type considered and for each of the three molecular profil-  
181 ing modalities, an optimal range of  $D$  and  $K$  parameters where the performance of inference was  
182 consistently high in the subset and only weakly dependent on these parameters (*Figure S1*). We  
183 then selected and used, for the remainder of the patients with this cancer type and for this profiling  
184 modality, a pair  $D$  and  $K$  values from within the optimal range. As an additional validation of our  
185 parameter optimization procedure, we applied it to a set of cancer-free WES profiles of TCGA-OV  
186 patients. Comparing the resulting ancestry calls to the consensus calls (C5) by TCGA (*Carrot-Zhang*  
187 *et al., 2020*), we find the two to be in excellent agreement *Table S3*.

188 We also assessed the cohort-wide performance of our ancestry calls from original cancer-derived  
189 molecular data, by comparison to the gold standard of ancestry as determined from the match-  
190 ing cancer-free genotypes. For Beat AML and TCGA-OV patients, we performed ancestry inference

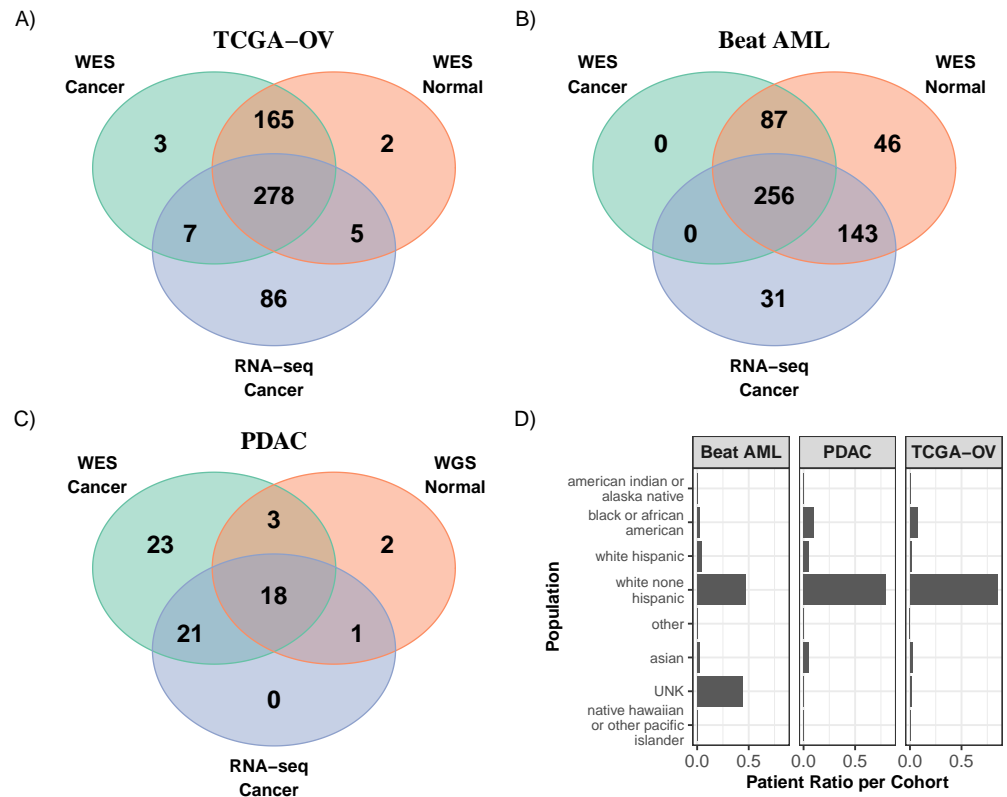


**Figure 2.** Summary of the molecular data used in this study. These originate from three patient cohorts: **A)** TCGA ovarian cancer **B)** acute myeloid leukemia and **C)** pancreatic ductal adenocarcinoma library of patient-derived organoids. **D)** The distribution of the patients by SIRE for Beat AML, PDAC and TCGA-OV cohorts. UNK means not reported or unknown.

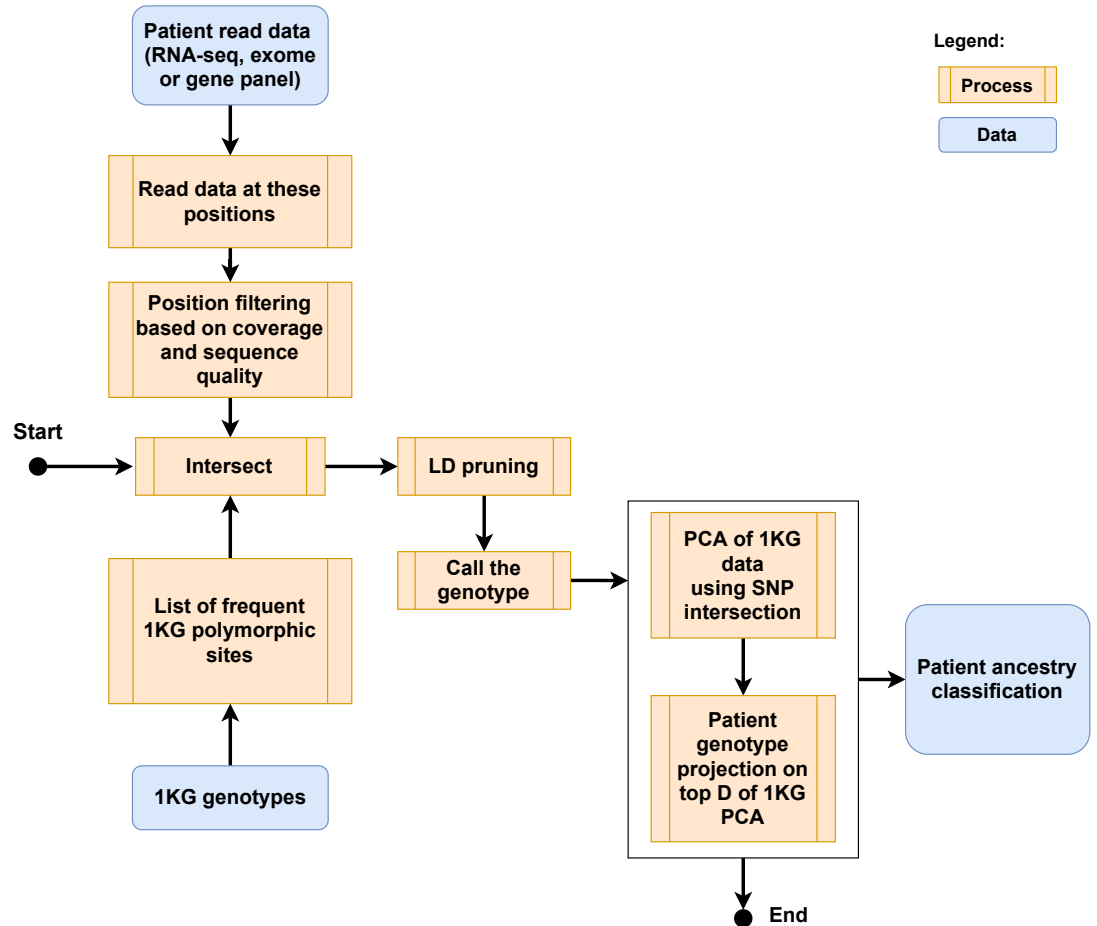


**Figure 3.** A flowchart of the inference of genetic ancestry.

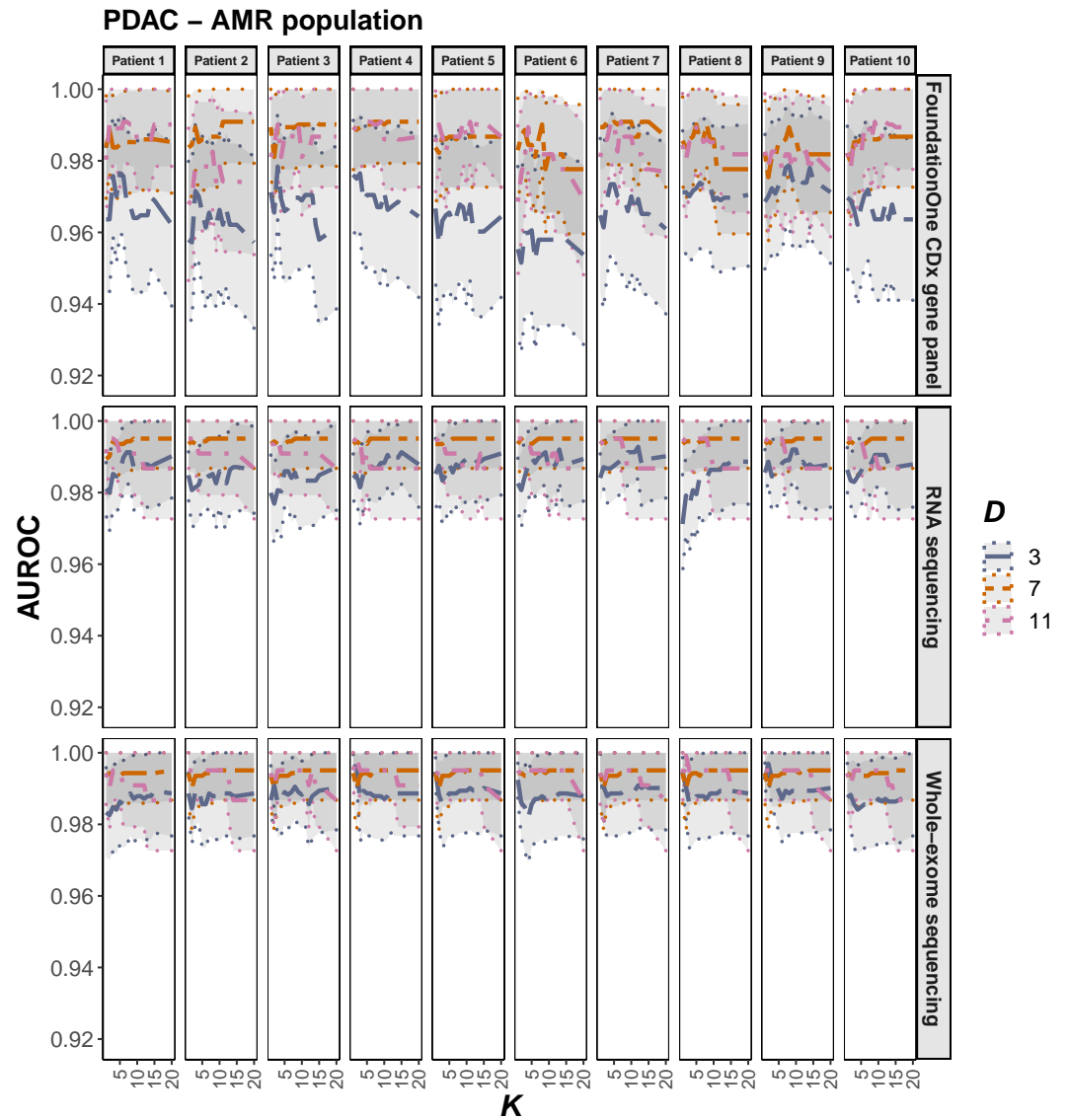


**Figure 4.** Dependence of AMR-specific AUROC on the inference parameters  $D$  and  $K$ , computed using data synthesis for 10 PDAC patients and the three profiling modalities: WES, RNA-seq and FoundationOne<sup>®</sup> CDx panels. The central AUROC values are shown in solid, and the 95% CI in dashed, lines.



Study	D	K	Accuracy	95% CI	AUROC	95% CI
TCGA-OV WES	5	13	0.998	0.994-1	0.993	0.992-0.994
TCGA-OV Panel	4	12	0.984	0.972-0.996	0.966	0.965-0.967
TCGA-OV RNA-seq	7	12	0.993	0.983-1	0.977	0.975-0.979
BeatAML WES	5	13	0.989	0.978-1	0.978	0.976-0.980
BeatAML Panel	4	13	0.991	0.981-1	0.999	0.999-0.999
BeatAML RNA-seq	4	13	0.992	0.981-1	0.999	0.999-0.999
PDAC WES	8	13	1	NA	NA	NA
PDAC Panel	6	5	0.952	0.861-1	0.958	NA
PDAC RNA-seq	4	13	1	NA	NA	NA

**Table 1.** Cohort-wide performance measures for super-population calls from cancer-derived molecular data, as compared to the matching cancer-free WES or (in the case of PDAC) WGS. A reliable estimate of the confidence intervals (CI) was not possible in the case of PDAC, due to the small number of cases with matching cancer-free genotypes.

191 from cancer-free patient exomes, using the same methodology as as we did for the cancer-derived  
192 sequences of these patients. In the case of PDAC, cancer-free whole-genome sequencing data were  
193 available, and used for the same purpose for a portion of the patient cohort. For all three cohorts,  
194 we summarize our cohort-wide findings in **Table 1** (we include similar tables for the synthetic data  
195 Table S9-S11). Ancestry calls from both microarray- and exome-derived genotypes were recently  
196 published by TCGA consortium (*Carrot-Zhang et al., 2020*), and we also used these so-called con-  
197 sensus (C5 in the following) calls in our performance assessment for TCGA-OV (Table S3).

198 We note that in the three patient cohorts we analyze here the sampling of patients with non-  
199 European ancestries is statistically insufficient for a purely cohort-based assessment of perfor-  
200 mance (**Table 2** and Table S5). We therefore report cohort-wide overall but not super-population  
201 specific AUROC values. Using data synthesis, we are able to compensate for this data shortfall  
202 in non-European ancestries and estimate super-population specific AUROC, as explained above  
203 (Tables S6,S7 and S8 and Figure S1).

204 The results of our analysis as presented in Tables S6,S7 and S8, lead to the following key observa-  
205 tions. First, we demonstrate a consistently high performance of our inference procedure across all  
206 cohorts and profiling modalities. Second, the super-population specific performance was the high-  
207 est for the European and both Asian super populations. The slightly lower accuracy as observed  
208 for the African and mixed American super-populations is likely due to a greater genetic variability  
209 within the African super-population and to a higher degree of (the predominantly European) ad-  
210 mixture in both super-populations. Third, the optimal choice of the *D*, *K* inference parameters, in  
211 general, depends on an individual cancer-derived molecular profile, even within the same cancer  
212 type and profiling modality (Figure S1 B,G,L).

213 In order to examine whether our inference procedure is robust against variation in the se-  
214 quence target coverage, we re-computed the ancestry calls for a subset of ten OV patients, with  
215 the cancer-derived whole-exome and RNA sequences of these patients down-sampled to between  
216 75% and 10% of the original coverage. The results, presented in (Figure S2) exhibit no substantial  
217 sensitivity of the inference accuracy to the depth of coverage in this range.

## 218 Discussion

219 With this work, we introduce a systematic approach to ancestry inference from cancer-derived  
220 molecular data. The approach is rooted in a combination of an established, extensively used PCA-  
221 based technique of ancestry inference with a central idea of inference parameter optimization us-  
222 ing data synthesized *in silico*. Crucially, this combination permits a statistically rigorous assessment  
223 of inference accuracy for an individual cancer-derived molecular profile, with its unique biological

(a) TCGA-OV WES

		Inferred				
pop		EAS	EUR	AFR	AMR	SAS
Cancer-free WES	EAS	10	0	0	0	0
	EUR	0	378	0	0	0
	AFR	0	0	29	0	0
	AMR	0	1	0	16	0
	SAS	0	0	0	0	7
	UNK	0	2	0	0	0

(b) BeatAML WES

		Inferred				
pop		EAS	EUR	AFR	AMR	SAS
Cancer-free WES	EAS	11	0	0	0	0
	EUR	0	283	0	6	0
	AFR	0	0	14	0	0
	AMR	0	0	0	27	0
	SAS	0	0	0	0	2
	UNK	0	0	0	0	0

(c) TCGA-OV Panel

		Inferred				
pop		EAS	EUR	AFR	AMR	SAS
Cancer-free WES	EAS	10	0	0	0	0
	EUR	0	376	0	2	0
	AFR	0	0	28	1	0
	AMR	0	4	0	13	0
	SAS	0	0	0	0	7
	UNK	0	2	0	0	0

(d) BeatAML Panel

		Inferred				
pop		EAS	EUR	AFR	AMR	SAS
Cancer-free WES	EAS	11	0	0	0	0
	EUR	0	286	0	3	0
	AFR	0	0	14	0	0
	AMR	0	0	0	27	0
	SAS	0	0	0	0	2
	UNK	0	0	0	0	0

(e) TCGA-OV RNA

		Inferred				
pop		EAS	EUR	AFR	AMR	SAS
Cancer-free WES	EAS	4	0	0	0	0
	EUR	0	242	0	0	0
	AFR	0	0	21	0	0
	AMR	1	1	0	9	0
	SAS	0	0	0	0	4
	UNK	0	1	0	0	0

(f) BeatAML RNA

		Inferred				
pop		EAS	EUR	AFR	AMR	SAS
Cancer-free WES	EAS	10	0	0	0	0
	EUR	0	210	0	2	0
	AFR	0	0	9	0	0
	AMR	0	0	0	24	0
	SAS	0	0	0	0	1
	UNK	0	0	0	0	0

**Table 2.** Confusion matrices comparing TCGA-OV or Beat AML patients' super-population calls from the cancer-derived molecular profiles for the three profiling modalities (rows) to those from the matching cancer-free WES.

224 (e.g. cancer type) and technical (e.g., sequencing depth and quality) properties. Synthetic data  
 225 here are used as a substitute for a real-world set of molecular profiles sharing these properties  
 226 and with known ground-truth genetic ancestry. It is unrealistic to expect such a real-world set to  
 227 be available in all cases. Our tests of the resulting computational methodology on a representative  
 228 subset of cancer-derived data demonstrate its accurate and robust performance. As we describe  
 229 in detail in the Methods section, our data synthesis method relies on heuristic components for an  
 230 estimate of the allele fractions throughout the cancer-derived profile. This estimate can be made  
 231 more rigorous by using haplotypes in future implementations of the method, but the present ver-  
 232 sion produces allele fractions in good agreement with published allele fractions (ASCAT2 results in  
 233 *(Grossman et al., 2016; NCI, 2021)*).

234 A line of research and development initiated with this work must be extended in several direc-  
 235 tions. First, the performance of the methods presented must be examined more comprehensively  
 236 across cancer types, and sequence properties, such as quality and depth. This task is computing-  
 237 intensive but feasible given extensive, well annotated repositories of cancer-derived data, such  
 238 as those resulting from TCGA Research Network (*Network, 2021*) and ICGC (*Zhang et al., 2019*)  
 239 projects. For these, the genetic ancestry of the patients either is known or can be readily es-

240 established using matching cancer-free molecular data. Second, an extension of our approach to  
241 additional profiling modalities should be examined. Chief among these are low-coverage whole-  
242 genome sequences commonly used for copy-number analysis and single-molecule, long-read se-  
243 quences. Each of these presents unique challenges and opportunities for the ancestry inference:  
244 in the former, the sparsity of coverage is compensated by its whole-genome breadth; in the lat-  
245 ter, the trade-off is between the high sequence error rate and the long-distance phasing afforded  
246 by long reads. Third, while the present work relied on PCA followed by nearest-neighbor classifi-  
247 cation for ancestry assessment, alternatives including UMAP for the former and Random Forest  
248 or Support Vector Machine for the latter exist and should be evaluated. Third, future method de-  
249 velopment should be extended beyond inference of global ancestry to that of local ancestry and  
250 ancestral admixture. Such an extension is particularly important in the study of cancer in strongly  
251 admixed populations, such as African and Latin Americans and may require more extensive refer-  
252 ence data, in addition to the 1KG reference used here. Finally, beyond cancer, our methodology  
253 can be applied to inference from genomic data originating in any kind of fragmentary or damaged  
254 nucleic-acid specimens, such as those encountered in forensic, archaeological or paleontological  
255 contexts.

256 We anticipate the computational approach described here to have a major, two-fold, impact  
257 on investigation of links between ancestry and cancer. First, it will become possible to massively  
258 boost the statistical power of such studies by leveraging existing tumor-derived molecular data  
259 sets without matching germline sequences or ancestry annotation. Our search of the Gene Ex-  
260 pression Omnibus (GEO) database alone has identified over 1,250 such data sets, containing RNA  
261 expression data for nearly 48,000 cancer tissue specimens. Such resources dwarf those of fully an-  
262 notated repositories, such as TCGA and International Cancer Genome Consortium (ICGC) (*Zhang*  
263 *et al.*, 2019). Other molecular data repositories are likely to contain resources of this category on a  
264 similar order of magnitude. Second, hundreds of thousands of tumor tissue specimens stored at  
265 multiple clinical centers constitute another major resource for ancestry-aware molecular studies of  
266 cancer. Here again, matching normal tissue specimens are often absent, and so is ethnic or racial  
267 annotation for the patients. According to a recent estimate (*Polubriaginof et al.*, 2019) such anno-  
268 tation is missing in electronic health records of over 50% of patients. Inferential tools presented  
269 here will make these massive resources of archival tissues available for ancestry-oriented cancer  
270 research.

## 271 **Methods and Materials**

### 272 **Data sets and pre-processing**

273 The data sets used in this work originate from three sources: TCGA collection for ovarian cystadeno-  
274 carcinoma (*The Cancer Genome Atlas Research Network*, 2011), Beat AML clinical trial (*Tyner et al.*,  
275 2018), and a study of pancreatic ductal adenocarcinoma (PDAC) using patient-derived organoids  
276 (*Tiriac et al.*, 2018). For all three, the data used are summarized, in the form of Venn diagrams and  
277 included cancer DNA (whole-exome or whole-genome) sequence, cancer RNA sequence and match-  
278 ing DNA (whole-exome or whole-genome) sequence. In all cases, read data mapped to the hg38  
279 version of the human genome were used. In order to study ancestry inference from targeted pan-  
280 els, the cancer-derived whole-exome data were reduced to reads mapping to the FoundationOne®  
281 CDx cancer-related gene panel (*INC*, 1999). Reads in the cancer-derived data were filtered for qual-  
282 ity using a cutoff phred score of 20. Following this filter, single-nucleotide substitutions were called  
283 at all positions with read coverage of at least 10, using Varscan version 2.4.4 (*Koboldt et al.*, 2013).  
284 This set of positions is called the high-confidence substitution (HCS) set in the following. From the  
285 1000 Genomes (1KG) variant call data in the Variant Call Format (VCF) (*Lowy-Gallego et al.*, 2019),  
286 genomic positions where substitution variants occur at a frequency of at least 0.01 in at least one  
287 of the super-populations comprising 1KG were selected as a basis for the ancestry inference. This  
288 set is referred to as the high-frequency substitution (HFS) set in the following. At the HFS positions

289 in the cancer-derived profile with the coverage above 10, the genotype was called. This set of po-  
290 sitions is referred to as high-confidence genotype (HCG) set in the following. In the HCG set, the  
291 total read count and the read counts for the reference and the alternative (according to HFS) alleles  
292 were determined. A genotype at an HCG position was considered undetermined if the excess of  
293 the total read count over the sum of the reference and alternative counts was inconsistent with the  
294 error of 0.001 at the  $p = 0.001$  level of significance. The same rule was used to call a heterozygous  
295 genotype. The HCG genomic positions were pruned to reduce correlation between neighboring  
296 genotypes using Bioconductor SNPRelate package version 1.22.0 (Zheng *et al.*, 2012), resulting in  
297 the pruned high-confidence genotype (PHCG) set of positions.

### 298 Ancestry inference

299 *Figure 3* lays out the workflow for ancestry inference. For a given cancer-derived profile, principal  
300 component analysis of the 1KG genotypes reduced to the PHCG was performed, and  $D$  top princi-  
301 pal components retained. The patient genotype reduced to PHCG was projected onto the subspace  
302 spanned by these  $D$  components. Within this subspace, the patient's ancestry was called as that of  
303 the 1KG super-population with the highest number of 1KG individuals among  $K$  nearest neighbors  
304 of the patient's genotype, using Euclidean distance in the  $D$ -dimensional subspace. If two or more  
305 super-populations were found tied in the nearest-neighbor count, no ancestry call was made for  
306 the patient. Only two such ties were observed in this work.

### 307 Measures of performance

308 We evaluate the performance of the ancestry inference by comparison to the ancestry inferred  
309 from the matching cancer-free data, wherever the latter are available. This is the case for the en-  
310 tirety of Beat AML and the OV data. For both, we infer the ancestry from the matching cancer-free  
311 exome profiles. In the case of OV data, we also compare the results to the consensus ancestry call  
312 (Carrot-Zhang *et al.*, 2020). In the case of PDAC matching cancer-free WGS data are available for  
313 22 patient cases (*Figure 2*), and our assessment of accuracy is based on this subset of the data. We  
314 compute, for each dataset, the  $5 \times 5$  confusion matrix (CM) for the 1KG superpopulation calls from  
315 the cancer-derived and cancer-free data sources. From the CM, the call accuracy is computed as  
316 the sum of the diagonal terms divided by that of the whole CM. Since the ancestral composition of  
317 all data sets considered here is heavily skewed towards the European super-population, we also  
318 compute the multi-class version of the area under the receiver operating characteristic curve (AU-  
319 ROC) (Hand and Till, 2001). AUROC is a measure of the call quality which compensates for the  
320 asymmetry in the class sizes. We use an R package pROC (CRAN version 1.16.2) (Robin *et al.*, 2011)  
321 for this purpose, and compute both the class-specific AUROC for each super-population and the  
322 5-class AUROC. In the class-specific case, we use a version DeLong's algorithm Sun and Xu (2014);  
323 DeLong *et al.* (1988) as implemented in the pROC package to compute the AUROC confidence in-  
324 tervals. In the 5-class case the confidence intervals are computed using bootstrap with 100-fold  
325 sampling.

### 326 Data synthesis

327 Data synthesis is defined here as replacement of the sequence variants detected in a cancer-  
328 derived profile  $P$  by those found in the genome of an unrelated individual  $U$ . Ingredients required  
329 for this procedure are: (a) allele fraction (AF) estimates in  $P$  and (b) the haplotype of  $U$  in the portion  
330 of the genome covered by  $P$ . With this knowledge, the procedure, depicted in *Figure 5*, consists  
331 of the following steps. First, sequence reads comprising  $P$  are distributed at random among the  
332 alleles with probabilities equal to the observed allele fractions. Second, in each haplotype block in  
333 the genome of  $U$  that is covered by  $P$ , allele assignment is made at random, yielding variant and  
334 reference read counts for each substitution in the genome of  $U$  within the scope of  $P$ .

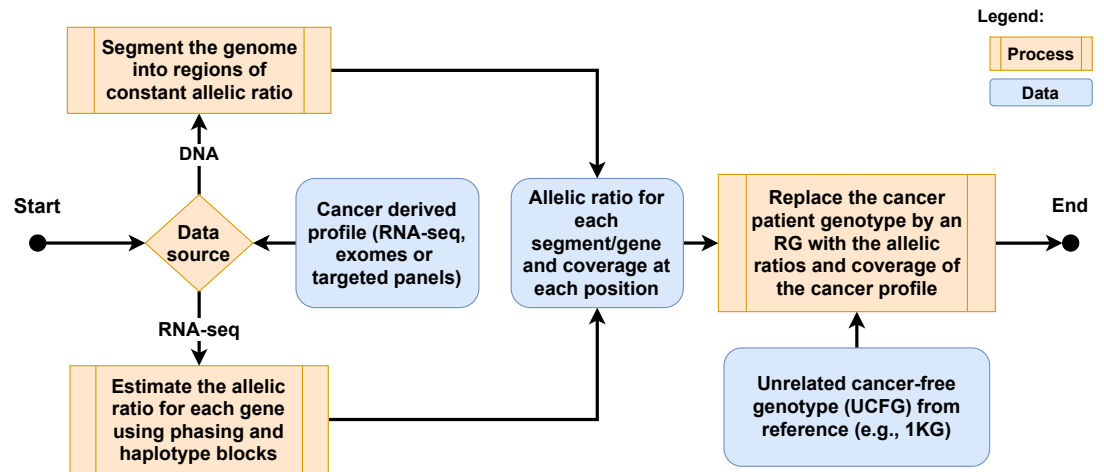


Figure 5. A schematic overview of the data synthesis process.

### 335 Inference parameter optimization using synthetic data

336 In order to optimize ancestry inference parameters  $D$  and  $K$  for a given cancer-derived molecular  
 337 profile, we generate a synthetic data set by repeatedly pairing the profile with 1KG genomes. A  
 338 subset of 780 1KG genomes is set aside for this purpose by drawing at random 30 genomes from  
 339 each of the 26 ancestral populations represented in 1KG. Genetic ancestry is then inferred for each  
 340 of the 780 synthetic profiles following the procedure described in the Ancestry Inference subsection,  
 341 each time with the 1KG genome used for synthesis removed from the reference data set.  
 342 The inference performance is then assessed as the 5-class AUROC, as explained in the Measures  
 343 of Performance subsection. AUROC is computed for the  $D, K$  pairs in a range of values of these  
 344 parameters, and the optimal  $D, K$  pairs yielding the highest accuracy are identified. Throughout  
 345 this work, AUROC was computed for all  $D$  and  $K$  in the rectangle  $3 \leq D \leq 11; 3 \leq K \leq 15$ . For all  
 346 combinations of data sources and profiling modalities considered, a set of  $D, K$  pairs was found  
 347 where the performance was optimal or differed from the optimum by no more than 3% (Figure 4).

### 348 Determination of allele fractions

349 As the Data Synthesis subsection makes clear, knowledge of allele fractions (AF) in a cancer-derived  
 350 profile is a prerequisite for data synthesis. We describe a 3-step AF estimate procedure which  
 351 relies exclusively on the cancer-derived molecular profile, in the absence of a matching cancer-free  
 352 genotype from the patient, as would be the case for the intended application of our methods. First  
 353 (step 1), the loss-of-heterozygosity (LOH) regions are delineated. Next (step 2), the regions of allele  
 354 imbalance where AF differs significantly from 1/2 are identified. Finally (step 3), AF are computed  
 355 throughout the regions of allele imbalance. These steps are implemented differently, depending  
 356 on whether the profile originates in the cancer DNA or RNA. We now discuss these steps, in turn  
 357 for the DNA- and the RNA-derived profiles (Figure S3).

For the DNA-derived profiles, the LOH regions (step 1) are detected as follows. An LOH region  
 in  $P$  must fit into a gap  $G$  between any two consecutive HCS positions, where all the observed  
 genotypes are consistent with homozygosity. Any region within  $G$  is then considered an LOH region  
 (see Figure S3 b) if it contains  $k_1$  PHCG positions with  $k_1 \geq k_{min}$  and for which the 1KG frequencies  
 $F_i, 1 \leq i \leq k_1$  of the alleles observed in the cancer-derived profile  $P$  satisfy

$$\log_{10} \left( \prod_{i=1}^{k_1} \frac{F_i^2}{\max [F_i^2, (1 - F_i)^2, 2F_i(1 - F_i)]} \right) < \lambda.$$

358 PHCG positions only are used for this purpose, to reduce correlations due to linkage. The values  
 359 of  $k_{min}$  and  $\lambda$  were chosen so as to maximize, in TCGA OV data set, the overlap between the regions  
 360 found to be LOH by these criteria and the published LOH regions ASCAT2 files from NCI's

361 Genomic Data Commons ((*Grossman et al., 2016; NCI, 2021*)). The latter were determined with full  
362 knowledge of the patient's cancer-free genotype. The optimal values were found to be  $k_{min} = 3$  and  
363  $\lambda = -3$ .

Step 2 is based on the notion of an "empty box" (see Figure S3 b). By this, we mean a contiguous region where the allele fraction of 1/2 is inconsistent with the read counts for the reference and alternative alleles at the HCS positions it contains. An empty box is constructed as follows. First, we consider sliding windows, each encompassing  $k_2$  consecutive HCS positions not separated by an LOH region. A window is called asymmetric if (a) for no less than  $k_2 - 1$  of the positions the minor allele count is outside the inner-quartile range (IQR) of the binomial distribution with the minor AF of  $f_0 = 1/2$  and (b) satisfy

$$\log_{10} \left( \prod_{i=1}^{k_2} \frac{2P_i}{(1 - 2P_i)} \right) < \lambda.$$

364 where  $P_i = P(X_i \leq \text{number of reads covering the minor allele at position } i)$  and,  $X_i$  is the binomial  
365 distribution with the number of trials equals the coverage at the position  $i$  and the probability of  
366 success  $\rho = 1/2$ . In this work,  $\lambda = -3$ . A polymorphic position is called asymmetric if it belongs  
367 to at least one asymmetric window. An empty box is a region with no less than  $k_2$  polymorphic  
368 positions, all of which are asymmetric. We used  $k_2 = 10$  throughout this work.

369 At step 3, in the case of DNA, we consider contiguous genome regions of allele asymmetry iden-  
370 tified at step 2. Each of these may consist of sub-regions with differing allele fractions. To detect  
371 these sub-regions, we "seed" the first sub-region with  $k_3$  HCS positions at the region's boundary  
372 and, in this window, estimate the minor allele fraction. We consider the adjacent window  $W$  of  
373  $k_3$  HCS positions  $k_3 + 1$  through  $2k_3$  and apply to it the empty box criteria as described for step 2,  
374 with  $f_0$  set to the estimated minor allele fraction of the first window. If the criteria are satisfied,  $W$   
375 becomes the seed of the next sub-region, and the process is repeated. Otherwise, HCS position  
376  $k_3 + 1$  is added the first sub-region and  $W$  is shifted to start at  $k_3 + 2$ , etc.

377 In the case of a cancer-derived RNA profile, the expressed allele fractions are, in general, gene  
378 specific. Therefore the steps 1 and 2 (condition b), as described above, are performed separately  
379 for each gene, assuming the minor allele fraction to be constant throughout the gene. Step 3 is  
380 then reduced to an empirical estimate of the minor allele fraction using read counts from all HCS  
381 positions within the gene.

### 382 Down-sampling of sequence data

383 In order to down-sample the sequence data to a desired fraction  $f$  of the original coverage, we sam-  
384 pled reads from the original patient profile  $P$  with the Bernoulli probability  $f$  without replacement.  
385 The ancestry inference procedure was then performed with the resulting sample of reads.

### 386 Schematic overviews and figures

387 All schematic overviews have been generated with draw.io version 15.7.3 (<http://www.diagrams.net>).

388 The Venn diagrams in *Figure 2* have been generated with CRAN packages VennDiagram version  
389 1.6.20 (*Chen, 2018*) and multipanelfigure version 2.1.2 (*Graumann and Cotton, 2018*).

390 The bar plot graph in *Figure 2* has been generated with CRAN package ggplot2 version 3.3.5  
391 (*Wickham, 2016*).

392 The AUROC graphs in *Figure 4* have been generated with CRAN packages ggplot2 version 3.3.5  
393 (*Wickham, 2016*) and cowplot version 1.1.1 (*Wilke, 2020*).

### 394 Acknowledgments

395 DAT is a distinguished scholar of the Lustgarten Foundation and Director of the Lustgarten Foundation-  
396 designated Laboratory of Pancreatic Cancer Research. DAT is also supported by the Cold Spring  
397 Harbor Laboratory Association, the New York Genome Center Polyethnic 1000 Project, the V Founda-  
398 tion (T2016-010), the Thompson Foundation, the Simons Foundation (552716), and the NIH

399 (P30CA45508, P20CA192996, U10CA180944, U01CA224013, U01CA210240, R01CA188134, R01CA249002,  
400 and R01CA229699). AK's work was supported by the New York Genome Center Polyethnic-1000  
401 Major Grant, Simons Foundation award # 519054, Lustgarten Foundation OPT2 project award  
402 and by the Simons Center for Quantitative Biology at Cold Spring Harbor Laboratory. This work  
403 was performed with assistance from the US National Institutes of Health Grant S10OD028632-01.  
404 The results published here are in part based upon data generated by TCGA Research Network:  
405 <https://www.cancer.gov/tcga>. We thank Adam Siepel, Lloyd Trotman, Jeffrey Boyd, W. Richard Mc-  
406 Combie, Thomas Gingeras, Justin Kinney, Camila dos Santos, Michael Schatz, Louis Staudt, Michael  
407 Berger, David Solit and Samuel Aparicio for illuminating discussions.

#### 408 **Authors' contributions**

409 PB and AK conceived the study. PB performed the data analysis with support of AK and AD. PB and  
410 AK wrote the manuscript with contributions from AD. PB and AD generated the figures. AK and  
411 DAT supervised the work and secured funding. All authors reviewed the manuscript.

#### 412 **Competing interests**

413 The authors declare that they have no competing interests.

#### 414 **References**

- 415 **Alexander DH**, Novembre J, Lange K. Fast model-based estimation of ancestry in unrelated indi-  
416 viduals. *Genome Res.* 2009; 19(9):1655–64. <https://www.ncbi.nlm.nih.gov/pubmed/19648217>, doi:  
417 [10.1101/gr.094052.109](https://doi.org/10.1101/gr.094052.109).
- 418 **Altshuler DL**, Durbin RM, Abecasis GR, Bentley DR, Chakravarti A, Clark AG, Collins FS, De La Vega FM, Don-  
419 nnelly P, Egholm M, Flicek P, Gabriel SB, Gibbs RA, Knoppers BM, Lander ES, Lehrach H, Mardis ER, McVean  
420 GA, Nickerson DA, Peltonen L, et al. A map of human genome variation from population-scale sequencing.  
421 *Nature.* 2010; 467(7319):1061–1073. doi: 10.1038/nature09534.
- 422 **Ashktorab H**, Kupfer SS, Brim H, Carethers JM. Racial Disparity in Gastrointestinal Cancer Risk.  
423 *Gastroenterology.* 2017; 153(4):910–923. <https://www.ncbi.nlm.nih.gov/pubmed/28807841>, doi:  
424 [10.1053/j.gastro.2017.08.018](https://doi.org/10.1053/j.gastro.2017.08.018).
- 425 **Barral-Arca R**, Pardo-Seco J, Bello X, Martinon-Torres F, Salas A. Ancestry patterns inferred from mas-  
426 sive RNA-seq data. *RNA.* 2019; 25(7):857–868. <https://www.ncbi.nlm.nih.gov/pubmed/31010885>, doi:  
427 [10.1261/rna.070052.118](https://doi.org/10.1261/rna.070052.118).
- 428 **Bhatnagar B**, Kohlschmidt J, Mrozek K, Zhao Q, Fisher JL, Nicolet D, Walker CJ, Mims AS, Oakes C, Giacomelli B,  
429 Orwick S, Boateng I, Blachly JS, Maharry SE, Carroll AJ, Powell BL, Kolitz JE, Stone RM, Byrd JC, Paskett ED, et al.  
430 Poor Survival and Differential Impact of Genetic Features of Black Patients with Acute Myeloid Leukemia.  
431 *Cancer Discov.* 2021; 11(3):626–637. <https://www.ncbi.nlm.nih.gov/pubmed/33277314>, doi: [10.1158/2159-  
432 8290.CD-20-1579](https://doi.org/10.1158/2159-8290.CD-20-1579).
- 433 **Carrot-Zhang J**, Chambwe N, Damrauer JS, Knijnenburg TA, Robertson AG, Yau C, Zhou W, Berger AC, Huang  
434 KL, Newberg JY, Mashl RJ, Romanel A, Sayaman RW, Demichelis F, Felau I, Frampton GM, Han S, Hoadley  
435 KA, Kemal A, Laird PW, et al. Comprehensive Analysis of Genetic Ancestry and Its Molecular Correlates  
436 in Cancer. *Cancer Cell.* 2020; 37(5):639–654 e6. <https://www.ncbi.nlm.nih.gov/pubmed/32396860>, doi:  
437 [10.1016/j.ccell.2020.04.012](https://doi.org/10.1016/j.ccell.2020.04.012).
- 438 **Carrot-Zhang J**, Soca-Chafre G, Patterson N, Thorner AR, Nag A, Watson J, Genovese G, Rodriguez J, Gelbard  
439 MK, Corrales-Rodriguez L, Mitsuishi Y, Ha G, Campbell JD, Oxnard GR, Arrieta O, Cardona AF, Gusev A, Mey-  
440 erson M. Genetic Ancestry Contributes to Somatic Mutations in Lung Cancers from Admixed Latin Ameri-  
441 can Populations. *Cancer Discov.* 2021; 11(3):591–598. <https://www.ncbi.nlm.nih.gov/pubmed/33268447>, doi:  
442 [10.1158/2159-8290.CD-20-1165](https://doi.org/10.1158/2159-8290.CD-20-1165).
- 443 **Chen H**. VennDiagram: Generate High-Resolution Venn and Euler Plots; 2018, [https://CRAN.R-project.org/  
444 package=VennDiagram](https://CRAN.R-project.org/package=VennDiagram), r package version 1.6.20.
- 445 **Cronin KA**, Lake AJ, Scott S, Sherman RL, Noone AM, Howlader N, Henley SJ, Anderson RN, Firth AU, Ma J, Kohler  
446 BA, Jemal A. Annual Report to the Nation on the Status of Cancer, part I: National cancer statistics. *Cancer.*  
447 2018; 124(13):2785–2800. <https://www.ncbi.nlm.nih.gov/pubmed/29786848>, doi: [10.1002/cncr.31551](https://doi.org/10.1002/cncr.31551).

- 448 **DeLong ER**, DeLong DM, Clarke-Pearson DL. Comparing the Areas under Two or More Correlated Receiver  
449 Operating Characteristic Curves: A Nonparametric Approach. *Biometrics*. 1988 jan; 44(3):837–845. <http://www.jstor.org/stable/2531595>, doi: 10.2307/2531595.
- 451 **Diaz-Papkovich A**, Anderson-Trocme L, Ben-Eghan C, Gravel S. UMAP reveals cryptic population structure and  
452 phenotype heterogeneity in large genomic cohorts. *PLoS Genetics*. 2019; 15(11):1–24. doi: 10.1371/jour-  
453 nal.pgen.1008432.
- 454 **Dutil J**, Chen Z, Monteiro AN, Teer JK, Eschrich SA. An Interactive Resource to Probe Genetic Diversity and  
455 Estimated Ancestry in Cancer Cell Lines. *Cancer Res*. 2019; 79(7):1263–1273. [https://www.ncbi.nlm.nih.gov/  
456 pubmed/30894373](https://www.ncbi.nlm.nih.gov/pubmed/30894373), doi: 10.1158/0008-5472.CAN-18-2747.
- 457 **Fairley S**, Lowy-Gallego E, Perry E, Flicek P. The International Genome Sample Resource (IGSR) collection of  
458 open human genomic variation resources. *Nucleic Acids Research*. 2019 10; 48(D1):D941–D947. [https://doi.  
459 org/10.1093/nar/gkz836](https://doi.org/10.1093/nar/gkz836), doi: 10.1093/nar/gkz836.
- 460 **Frampton GM**, Fichtenholtz A, Otto GA, Wang K, Downing SR, He J, Schnall-Levin M, White J, Sanford EM, An P,  
461 Sun J, Juhn F, Brennan K, Iwanik K, Maillet A, Buell J, White E, Zhao M, Balasubramanian S, Terzic S, et al.  
462 Development and validation of a clinical cancer genomic profiling test based on massively parallel DNA  
463 sequencing. *Nat Biotechnol*. 2013; 31(11):1023–31. <https://www.ncbi.nlm.nih.gov/pubmed/24142049>, doi:  
464 10.1038/nbt.2696.
- 465 **Graumann J**, Cotton R. multipanelfigure: Simple Assembly of Multiple Plots and Images into a Compound  
466 Figure. *Journal of Statistical Software, Code Snippets*. 2018; 84(3):1–10. doi: 10.18637/jss.v084.c03.
- 467 **Grossman RL**, Heath AP, Ferretti V, Varmus HE, Lowy DR, Kibbe WA, Staudt LM. Toward a Shared Vision for Cancer  
468 Genomic Data. *The New England journal of medicine*. 2016 sep; 375(12):1109–1112. [https://pubmed.ncbi.  
469 nlm.nih.gov/27653561](https://pubmed.ncbi.nlm.nih.gov/27653561)<https://www.ncbi.nlm.nih.gov/pmc/articles/PMC6309165/>, doi: 10.1056/NEJMp1607591.
- 470 **Hand DJ**, Till RJ. A Simple Generalisation of the Area Under the ROC Curve for Multiple Class Classification  
471 Problems. *Machine Learning*. 2001; 45(2):171–186. doi: 10.1023/A:1010920819831.
- 472 **Huang BZ**, Stram DO, Le Marchand L, Haiman CA, Wilkens LR, Pandol SJ, Zhang ZF, Monroe KR, Setiawan VW.  
473 Interethnic differences in pancreatic cancer incidence and risk factors: The Multiethnic Cohort. *Cancer Med*.  
474 2019; 8(7):3592–3603. <https://www.ncbi.nlm.nih.gov/pubmed/31066497>, doi: 10.1002/cam4.2209.
- 475 **Huang Q**, Baudis M. Enabling population assignment from cancer genomes with SNP2pop. *Sci Rep*. 2020;  
476 10(1):4846. <https://www.ncbi.nlm.nih.gov/pubmed/32179800>, doi: 10.1038/s41598-020-61854-x.
- 477 **INC FM**, FoundationOne Liquid CDx; 1999. [https://assets.ctfassets.net/w98cd481qyp0/  
478 YqqKHaqQmFqc5ueQk48w/c35460768c3a76ef738dcf88f8219524/F1CDx\\_Tech\\_Specs\\_072021.pdf](https://assets.ctfassets.net/w98cd481qyp0/YqqKHaqQmFqc5ueQk48w/c35460768c3a76ef738dcf88f8219524/F1CDx_Tech_Specs_072021.pdf).
- 479 **Kessler MD**, Bateman NW, Conrads TP, Maxwell GL, Dunning Hotopp JC, O'Connor TD. Ancestral characteriza-  
480 tion of 1018 cancer cell lines highlights disparities and reveals gene expression and mutational differences.  
481 *Cancer*. 2019; 125(12):2076–2088. <https://www.ncbi.nlm.nih.gov/pubmed/30865299>, doi: 10.1002/cncr.32020.
- 482 **Koboldt DC**, Larson DE, Wilson RK. Using VarScan 2 for Germline Variant Calling and Somatic Mutation De-  
483 tection. *Current Protocols in Bioinformatics*. 2013 dec; 44(1). [https://onlinelibrary.wiley.com/doi/10.1002/  
484 0471250953.bi1504s44](https://onlinelibrary.wiley.com/doi/10.1002/0471250953.bi1504s44), doi: 10.1002/0471250953.bi1504s44.
- 485 **Lowy-Gallego E**, Fairley S, Zheng-Bradley X, Ruffier M, Clarke L, Flicek P. Variant calling on the GRCh38 as-  
486 sembly with the data from phase three of the 1000 Genomes Project. *Wellcome Open Research*. 2019 dec;  
487 4:50. <https://pubmed.ncbi.nlm.nih.gov/32175479>[https://www.ncbi.nlm.nih.gov/pmc/articles/PMC7059836/  
488 https://wellcomeopenresearch.org/articles/4-50/v2](https://www.ncbi.nlm.nih.gov/pmc/articles/PMC7059836/), doi: 10.12688/wellcomeopenres.15126.2.
- 489 **Mahal BA**, Alshalalfa M, Kensler KH, Chowdhury-Paulino I, Kantoff P, Mucci LA, Schaeffer EM, Spratt D, Yamoah  
490 K, Nguyen PL, Rebbeck TR. Racial Differences in Genomic Profiling of Prostate Cancer. *N Engl J Med*. 2020;  
491 383(11):1083–1085. <https://www.ncbi.nlm.nih.gov/pubmed/32905685>, doi: 10.1056/NEJMc2000069.
- 492 **Mersha TB**, Abebe T. Self-reported race/ethnicity in the age of genomic research: its potential impact on  
493 understanding health disparities. *Human Genomics*. 2015; 9(1):1. <https://doi.org/10.1186/s40246-014-0023-x>,  
494 doi: 10.1186/s40246-014-0023-x.
- 495 **NCI**, National Cancer Institute, Genomic Data Commons; 2021. <https://gdc.cancer.gov/>.
- 496 **Network TR**, TCGA Research Network; 2021. [https://www.cancer.gov/about-nci/organization/ccg/research/  
497 structural-genomics/tcga](https://www.cancer.gov/about-nci/organization/ccg/research/structural-genomics/tcga).



- 498 **Nugent A**, Conatser KR, Turner LL, Nugent JT, Sarino EMB, Ricks-Santi LJ. Reporting of race in genome and  
499 exome sequencing studies of cancer: a scoping review of the literature. *Genet Med*. 2019; 21(12):2676–2680.  
500 <https://www.ncbi.nlm.nih.gov/pubmed/31160752>, doi: 10.1038/s41436-019-0558-2.
- 501 **Polubriaginof FCG**, Ryan P, Salmasian H, Shapiro AW, Perotte A, Safford MM, Hripcsak G, Smith S, Tatonetti  
502 NP, Vawdrey DK. Challenges with quality of race and ethnicity data in observational databases. *Journal of*  
503 *the American Medical Informatics Association*. 2019 aug; 26(8-9):730–736. [https://academic.oup.com/jamia/](https://academic.oup.com/jamia/article/26/8-9/730/5542028)  
504 [article/26/8-9/730/5542028](https://academic.oup.com/jamia/article/26/8-9/730/5542028), doi: 10.1093/jamia/ocz113.
- 505 **Price AL**, Patterson NJ, Plenge RM, Weinblatt ME, Shadick NA, Reich D. Principal components analysis corrects  
506 for stratification in genome-wide association studies. *Nat Genet*. 2006; 38(8):904–9. [https://www.ncbi.nlm.](https://www.ncbi.nlm.nih.gov/pubmed/16862161)  
507 [nih.gov/pubmed/16862161](https://www.ncbi.nlm.nih.gov/pubmed/16862161), doi: 10.1038/ng1847.
- 508 **Pritchard JK**, Stephens M, Donnelly P. Inference of population structure using multilocus genotype data. *Ge-*  
509 *netics*. 2000; 155(2):945–59. <https://www.ncbi.nlm.nih.gov/pubmed/10835412>.
- 510 **Robin X**, Turck N, Hainard A, Tiberti N, Lisacek F, Sanchez JC, Müller M. pROC: an open-source package for R and  
511 S+ to analyze and compare ROC curves. *BMC Bioinformatics*. 2011 dec; 12(1):77. [https://bmcbioinformatics.](https://bmcbioinformatics.biomedcentral.com/articles/10.1186/1471-2105-12-77)  
512 [biomedcentral.com/articles/10.1186/1471-2105-12-77](https://bmcbioinformatics.biomedcentral.com/articles/10.1186/1471-2105-12-77), doi: 10.1186/1471-2105-12-77.
- 513 **Siegel RL**, Miller KD, Jemal A. Cancer statistics, 2020. *CA Cancer J Clin*. 2020; 70(1):7–30. [https://www.ncbi.nlm.](https://www.ncbi.nlm.nih.gov/pubmed/31912902)  
514 [nih.gov/pubmed/31912902](https://www.ncbi.nlm.nih.gov/pubmed/31912902), doi: 10.3322/caac.21590.
- 515 **Sinha S**, Mitchell KA, Zingone A, Bowman E, Sinha N, Schäffer AA, Lee JS, Ruppin E, Ryan BM. Higher prevalence  
516 of homologous recombination deficiency in tumors from African Americans versus European Americans.  
517 *Nature Cancer*. 2020; 1(1):112–121. <https://doi.org/10.1038/s43018-019-0009-7>, doi: 10.1038/s43018-019-  
518 0009-7.
- 519 **Sun X**, Xu W. Fast Implementation of DeLong’s Algorithm for Comparing the Areas Under Correlated Re-  
520 ceiver Operating Characteristic Curves. *IEEE Signal Processing Letters*. 2014 nov; 21(11):1389–1393. [http:](http://ieeexplore.ieee.org/document/6851192/)  
521 [//ieeexplore.ieee.org/document/6851192/](http://ieeexplore.ieee.org/document/6851192/), doi: 10.1109/LSP.2014.2337313.
- 522 **Tan DS**, Mok TS, Rebbeck TR. Cancer Genomics: Diversity and Disparity Across Ethnicity and Geography. *J Clin*  
523 *Oncol*. 2016; 34(1):91–101. <https://www.ncbi.nlm.nih.gov/pubmed/26578615>, doi: 10.1200/JCO.2015.62.0096.
- 524 **Tate JG**, Bamford S, Jubb HC, Sondka Z, Beare DM, Bindal N, Boutselakis H, Cole CG, Creatore C, Dawson E,  
525 Fish P, Harsha B, Hathaway C, Jupe SC, Kok CY, Noble K, Ponting L, Ramshaw CC, Rye CE, Speedy HE, et al.  
526 COSMIC: the Catalogue Of Somatic Mutations In Cancer. *Nucleic Acids Research*. 2018 10; 47(D1):D941–D947.  
527 <https://doi.org/10.1093/nar/gky1015>, doi: 10.1093/nar/gky1015.
- 528 **The Cancer Genome Atlas Research Network**. Integrated genomic analyses of ovarian carcinoma. *Nature*.  
529 2011 jun; 474(7353):609–615. <http://www.nature.com/articles/nature10166>, doi: 10.1038/nature10166.
- 530 **Tiriac H**, Belleau P, Engle DD, Plenker D, Deschênes A, Somerville TDD, Froeling FEM, Burkhart RA, Denroche  
531 RE, Jang GH, Miyabayashi K, Young CM, Patel H, Ma M, LaComb JF, Palmaira RLD, Javed AA, Huynh JC, John-  
532 son M, Arora K, et al. Organoid Profiling Identifies Common Responders to Chemotherapy in Pancreatic  
533 Cancer. *Cancer Discovery*. 2018 sep; 8(9):1112–1129. <https://www.ncbi.nlm.nih.gov/pubmed/29853643>[http:](http://cancerdiscovery.aacrjournals.org/lookup/doi/10.1158/2159-8290.CD-18-0349)  
534 [//cancerdiscovery.aacrjournals.org/lookup/doi/10.1158/2159-8290.CD-18-0349](http://cancerdiscovery.aacrjournals.org/lookup/doi/10.1158/2159-8290.CD-18-0349), doi: 10.1158/2159-8290.CD-18-  
535 0349.
- 536 **Tyner JW**, Tognon CE, Bottomly D, Wilmot B, Kurtz SE, Savage SL, Long N, Schultz AR, Traer E, Abel M, Agarwal A,  
537 Blucher A, Borate U, Bryant J, Burke R, Carlos A, Carpenter R, Carroll J, Chang BH, Coblenz C, et al. Functional  
538 genomic landscape of acute myeloid leukaemia. *Nature*. 2018; 562(7728):526–531. [https://www.ncbi.nlm.nih.](https://www.ncbi.nlm.nih.gov/pubmed/30333627)  
539 [gov/pubmed/30333627](https://www.ncbi.nlm.nih.gov/pubmed/30333627), doi: 10.1038/s41586-018-0623-z.
- 540 **Wickham H**. *ggplot2: Elegant Graphics for Data Analysis*. Springer-Verlag New York; 2016. [https://ggplot2.](https://ggplot2.tidyverse.org)  
541 [tidyverse.org](https://ggplot2.tidyverse.org).
- 542 **Wilke CO**. cowplot: Streamlined Plot Theme and Plot Annotations for ‘ggplot2’; 2020, [https://CRAN.R-project.](https://CRAN.R-project.org/package=cowplot)  
543 [org/package=cowplot](https://CRAN.R-project.org/package=cowplot), r package version 1.1.1.
- 544 **Yuan J**, Hu Z, Mahal BA, Zhao SD, Kensler KH, Pi J, Hu X, Zhang Y, Wang Y, Jiang J, Li C, Zhong X, Montone KT,  
545 Guan G, Tanyi JL, Fan Y, Xu X, Morgan MA, Long M, Zhang Y, et al. Integrated Analysis of Genetic Ancestry  
546 and Genomic Alterations across Cancers. *Cancer Cell*. 2018; 34(4):549–560 e9. [https://www.ncbi.nlm.nih.gov/](https://www.ncbi.nlm.nih.gov/pubmed/30300578)  
547 [pubmed/30300578](https://www.ncbi.nlm.nih.gov/pubmed/30300578), doi: 10.1016/j.ccell.2018.08.019.

- 548 **Zhang J**, Bajari R, Andric D, Gerthoffert F, Lepsa A, Nahal-Bose H, Stein LD, Ferretti V. The International Cancer  
549 Genome Consortium Data Portal. *Nature Biotechnology*. 2019 apr; 37(4):367–369. [http://www.nature.com/  
550 articles/s41587-019-0055-9](http://www.nature.com/articles/s41587-019-0055-9), doi: 10.1038/s41587-019-0055-9.
- 551 **Zheng X**, Levine D, Shen J, Gogarten SM, Laurie C, Weir BS. A high-performance computing toolset for  
552 relatedness and principal component analysis of SNP data. *Bioinformatics*. 2012 10; 28(24):3326–3328.  
553 <https://doi.org/10.1093/bioinformatics/bts606>, doi: 10.1093/bioinformatics/bts606.